applied sciences

MDPI

Article

Examination of Efficient Operation Method of ATES System by Comparison Operation with WTES System of Existent Heat Storage System

Jewon Oh [1], Daisuke Sumiyoshi [2], Masatoshi Nishioka [3] and Hyunbae Kim [4,*]

1 Artificial Intelligence Applied Research Institute, Kurume Institute of Technology, 2228-66 Kamitsu-machi, Kurume, Fukuoka 830-0052, Japan; ohjewon@kurume-it.ac.jp
2 Department of Architecture, Kyushu University, 744 Motooka, Nishi-ku, Fukuoka 819-0395, Japan; sumiyoshi@arch.kyushu-u.ac.jp
3 Graduate School of Engineering, Osaka City University, 3-3-138 Sugimoto, Sugimoto-ku, Osaka 588-8585, Japan; nishioka@eng.osaka-cu.ac.jp
4 Graduate School of Agricultural and Life Sciences, The University of Tokyo, 1-1-1, Yayoi, Bunkyo-ku, Tokyo 113-8657, Japan
* Correspondence: hyunbae.kim27@gmail.com

Abstract: Aquifer thermal energy storage (ATES) system is widely used mainly in Europe and USA. In this paper, we examined the efficient operation method of ATES by comparing it with the water thermal energy storage (WTES) system of an existent thermal energy storage (TES) system using simulation. This study uses three aquifers: pumping wells, thermal storage wells, and reducing wells. The initial temperature is 19.1 °C groundwater from the surrounding area. ATES systems use the same operating methods as WTES systems to reduce heat storage efficiency and increase energy consumption. The operation that combines the ATES system with the pre-cooling/pre-heating coil can be used for air conditioning operation even if the heat storage diffuses or the pumping temperature changes. The aquifer heat storage system was used for the pre-cooling/pre-heating coil, and the cooling power consumption was reduced by 20%. The heating operation could not maintain heat for a long time due to the influence of groundwater flowing in from the surroundings. Therefore, it is recommended to use the stored heat as soon as possible. When energy saving is important by introducing a pre-cooling/pre-heating coil, the operation is performed by storing heat at a low temperature close to geothermal heat and also using groundwater heat. In addition, if the reduction of peak power in the daytime is important, it is appropriate to operate so that the heat stored in the pre-cooling/pre-heating coil is used up as much as possible. As a result, it was found that it is effective to operate the ATES system in combination with a pre-cooling/pre-heating coil. In cooling operation, ATES-C1-7 was the lowest at coefficient of performance (COP) 2.4 and ATES-C2-14 was the highest at COP 3.7. In heating operation, ATES-H1-45 was the lowest at COP1.2, and in other cases, it was about the same at COP2.4-2.8. In terms of energy efficiency, the heating operation ATES-H1-45 had a low energy efficiency of 4.1 for energy efficiency ratio (EER) and 3.9 for seasonal energy efficiency ratio (SEER). In other cases, the energy efficiency was 8.2–12.4 for EER and 8.7–15.3 for SEER.

Keywords: aquifer thermal energy storage system; water thermal energy storage system; efficient operation method; water-cooled heat pump; simulation analysis; pre-cooling/pre-heating coil

Citation: Oh, J.; Sumiyoshi, D.; Nishioka, M.; Kim, H. Examination of Efficient Operation Method of ATES System by Comparison Operation with WTES System of Existent Heat Storage System. *Appl. Sci.* **2021**, *11*, 10321. https://doi.org/10.3390/app112110321

Academic Editors: Birm-June Kim and Sumin Kim

Received: 6 September 2021
Accepted: 29 October 2021
Published: 3 November 2021

1. Introduction

Reducing greenhouse gas emissions is an urgent issue as a measure against global warming [1]. To solve the problem, it is indispensable to introduce a large amount of renewable energy such as solar power generation and wind power generation [2–4]. However, the mass introduction of renewable energy makes it difficult to balance the power

system. It has also been pointed out that restrictions on the power system are becoming apparent, such as surplus power generated during the interim period when power demand is low. Energy management that includes time shifts, such as dispersion of power demand in consideration of the balance between power supply and demand is required [5,6]. Xu et al. [2] analyzed how to use solar energy efficiently. In the future, it is necessary to analyze the optimal operation method for technical and economics. Palensky et al. [5] analyzed the demand-side management (DSM) overview and provided the optimal solution. Lund et al. [3,6] examined renewable energy optimal operation such as wind power and photovoltaic (PV) in Denmark, and proposed optimal systems for efficient energy supply. These previous studies have not examined the introduction of a heat storage system. In the future, the introduction of power storage systems and heat storage systems is expected [7–9]. The introduction of a power storage system is considered to be an effective solution, but there are still many problems in terms of installation cost and energy loss [10,11]. Under these circumstances, attention to heat storage systems is regaining attention. Until now, heat storage systems have aimed to save costs by storing cold and hot heat for air conditioning with inexpensive electricity at night and using it in the daytime. In the future, the surplus electricity in the daytime will be used to store cold and hot heat for air conditioning and will be used during cloudy hours and at night when sufficient electricity from sunlight cannot be obtained [12,13]. Therefore, it is expected to work as an adjustment device that shifts the time of power supply and demand [14].

Water thermal energy storage (WTES) systems are the most widespread and serve the function of adjusting electric power [15]. The WTES system has been introduced to reduce power consumption during peak hours in the daytime by using it as a daily heat storage system that stores heat at night and dissipates heat in the daytime [16]. In addition, since the heat source machine can be operated at full load operation at night and heat can be stored in a short time, the efficiency of the heat source equipment can be improved and the operating time of the heat source primary pump can be reduced. In some cases, energy saving can be achieved [17]. On the other hand, aquifer thermal energy storage (ATES) systems that store heat in strata surrounded by groundwater such as sand layers, which have relatively high permeability in the ground, are beginning to spread mainly in Europe and the United States [18–20]. Similar to the conventional WTES system, this system stores cold and hot water at night and performs heat utilization operations in the daytime. In addition, it stores hot heat in summer and uses it in winter. It is also possible to directly use the groundwater in the aquifer.

The ATES system and the WTES system also use water as a heat source. In the WTES system, a tank is installed in the underground space of the building to store heat and dissipate heat. The ATES system performs heat storage and heat utilization operation for underground strata. The ATES system has a larger capacity than the WTES system and has the advantage of using geothermal heat. Disadvantages include heat loss due to groundwater and the presence or absence of an aquifer. The ATES system can be expected as a measure against the heat island. However, it is important to manage the groundwater because it uses the groundwater directly. The difference between the ATES system and the geothermal system is the method of burying pipes to directly utilize the heat of the ground and the heat of the groundwater.

Ghaebi et al. [21] used a simulation to study an energy-saving operation method for an air-conditioning system that combines an ATES system and solar heat for an apartment house. Vanhoudt et al. [22], Paksoy et al. [23] compared the ATES system with the existing air conditioning system for hospitals using experiments and simulations. As a result, it was reported that the primary energy consumption could be reduced by 71% by using the ATES system. Picone et al. [24] reported that experiments and simulations could be used to combine solar heat with the ATES system to improve the heat recovery of the ATES system. Paksoy et al. [25], Karim et al. [26] used simulations to deploy ATES systems in commercial facilities, universities, office buildings, etc. to analyze electricity energy. During cooling operation, energy can be reduced by 60–80% and peak power can be suppressed

by 80–90%. We were able to reduce primary energy by 20–30% during heating operation. Nakamura et al. [27,28] used experiments to Improve the heat recovery rate of heat storage wells to 90% by installing impermeable walls on the ground for a 40% low-efficiency aquifer. Umemiya et al. [29,30] improved the heat recovery rate to 60% by applying a heat-insulating material to the pump pipe to the aquifer with a heat recovery rate of 23% throughout the experiment. This is due to the heat loss of the pipe. Nakaso et al. [31,32] constructed a simple cylindrical lumped constant model using the basic equation of FEFLOW [33] and verified the accuracy of the model by comparing it with the experimental values. Kitaoka et al. [34], Ochito et al. [35,36] clarified the characteristics of the ATES system in the short and long term by three-dimensional permeation/consolidation coupled analysis simulation and actual measurement survey using three heat storage wells. In these previous studies, the performance and potential of the ATES system have been mainly verified. However, no research has been conducted on operating methods and control methods according to the operating conditions of the aquifer heat storage system.

The purpose of this study is to clarify the efficient operation method by comparing the operating performance of the ATES system with that of the WTES system. We will examine an efficient operation method of the ATES system by comparing the operation control of the ATES system and the change of the heat storage set temperature with the WTES system. In this study, we use the building and energy management system (BEMS) to collect the outside air temperature, secondary heat load, power consumption, etc. In addition, we are conducting demonstration experiments and acquiring data such as the temperature inside the aquifer, water injection, and pumping flow rates. Model parameters and accuracy are verified using these data. We will clarify the efficient operation method through simulation of the operating performance of the ATES system.

2. Simulation Model and Calculation Method

This model was constructed using Visual Basic 2017, such as a WTES system, ATES system, water-cooled heat pump (water-cooled HP), and air handling unit (AHU). The calculation time interval is 1 min, and the input values are the outside air temperature, the load on the secondary side, and the cooling water temperature for each time.

2.1. WTES System Model

The WTES system model is as shown in Appendix A. Figure 1 shows a conceptual diagram of the WTES system model. Table 1 shows the WTES system model settings. The WTES system used temperature stratified storage tank models from Niwa et al. [37], Sagara et al. [38]. This model divides the entire heat storage tank into N layers of equal capacity and resolves heat transfer between layers. The WTES system model is calculated by dividing the heat accumulator capacity into 10 layers assuming a tank capacity of 1000 m^3. The heat accumulator tank is assumed to be a horizontally spreading water tank with a height of 3 m. The initial temperature of the heat storage tank is 15 °C. The operation control of the WTES system is performed as follows. The heat storage operation for cooling is performed when the ninth layer temperature is below 10 °C. When the temperature of the eighth layer reaches 8 °C or higher, the heat storage operation is stopped. The heat utilization operation is performed when the temperature of the third layer is 8 °C or lower. The heat utilization operation is stopped when the temperature of the eighth layer is 11 °C or higher. The heat storage operation for heating is performed when the temperature of the ninth layer is 42 °C or lower. The heat storage operation is stopped when the eighth layer temperature is above 44 °C. For the heat utilization operation, the heat utilization operation is performed when the temperature of the third layer is 41 °C or higher. The heat utilization operation stops when the eighth layer temperature is below 42 °C.

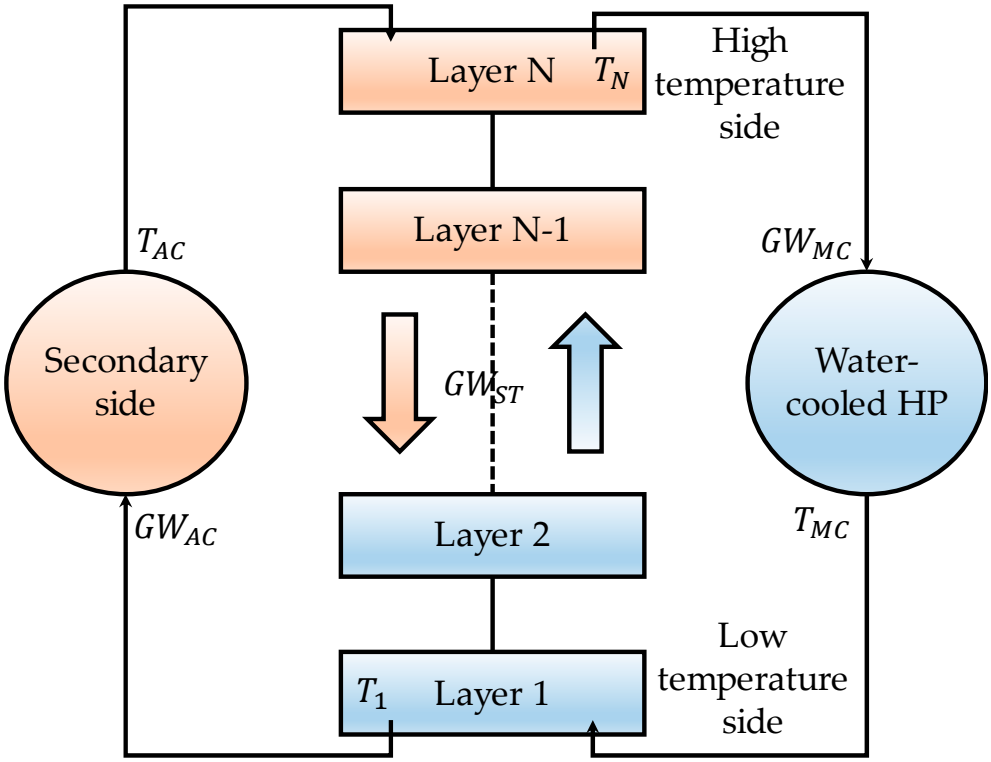

Figure 1. The stratum diagram of the heat storage well. GW_AC is flow rate from secondary side [m^3/h], GW_MC is flow rate from water-cooled HP [m^3/h], GW_ST is flow rate between layers [m^3/h], T_AC is inflow temperature from secondary side [°C], T_MC is inflow temperature from heat source [°C], T_1 is temperature of layer 1 [°C], and T_N is temperature of layer N [°C].

Table 1. The WTES system model settings.

Heat storage tank capacity [m^3]			1000
Number of layers [-]			10
Inflow flow rate [L/min]			833
Inflow temperature [°C]			Cooling: 7 Heating: 45
Initial temperature in the heat storage tank [°C]			15
Cooling	Heat storage operation	start	The 9th layer is below 10 °C
		Stop	8th layer 8 °C or more
	Heat utilization operation	start	The third layer is below 8 °C
		Stop	8th layer 11 °C or higher
Heating	Heat storage operation	start	The 9th layer is below 42 °C
		Stop	8th layer 44 °C or higher
	Heat utilization operation	start	The third layer is below 41 °C
		Stop	8th layer 42 °C or higher

2.2. ATES System Model

The ATES system model is as shown in Appendix B. The aquifer model was created based on the cylindrical model of Nakaso et al. [32] and the energy equation in FEFLOW [33]. Figure 2 shows a conceptual diagram of the cylindrical model. In this model, assuming that the upper and lower parts are horizontal aquifers under pressure and sandwiched between impermeable layers. The groundwater flow velocity between

layers is set to 0 m/s, and the heat transfer due to groundwater transfer is calculated. Then, consider the heat loss due to heat conduction include the inner and outer layers. The outer edge (boundary) of the cylinder of the aquifer is opened and flows out from the outer edge by water injection to lose heat. In the pumping operation, groundwater at underground temperature flows in from the outer edge. The parameters of the ATES system model were established using experimental data. The parameter was set by examining the thickness of the impermeable layer [39].

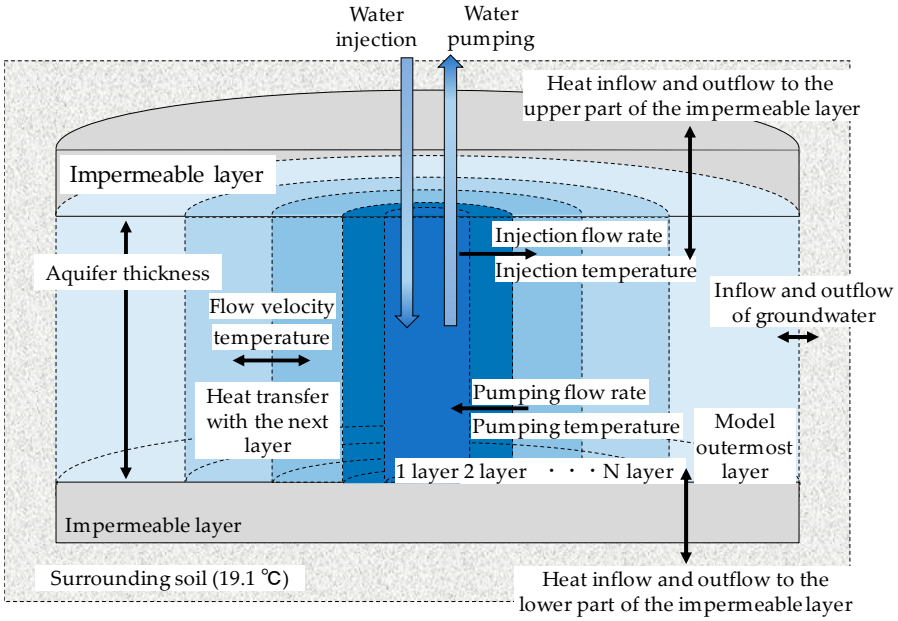

Figure 2. A conceptual diagram of the cylindrical model.

Figure 3 shows a geological map in which the ATES system was actually installed. The ATES system operates using three wells: a pumping well (6 m), a heat storage well (22 m–32 m), and a reduction well (80 m). The pumping and heat storage wells are sand gravel layers. The reduction wells are clay mixed sand and gravel layers. The excavation depth of the heat storage well is located between GL-22 m and GL-32 m. The ground of the heat storage well is a clay layer of the impermeable layer from GL-32 m, but the upper part of the heat storage well is a gravel layer in the water-permeable layer. The diameter of the well is 0.45 m, and the strainer position is GL-22 m to −30 m. The submersible pump is located at GL-22 m, and temperature sensors are installed at a total of five locations. The water pumped from the pumping well exchanges heat with the hot water sent from the heat pumps through a heat exchanger, and stores the heat in the heat storage well. The heat stored in the heat storage well is pumped up and sent to the air handling unit (AHU) installed in the building to perform heat utilization operation. It is a system that returns water to the reduction well after heat utilization operation.

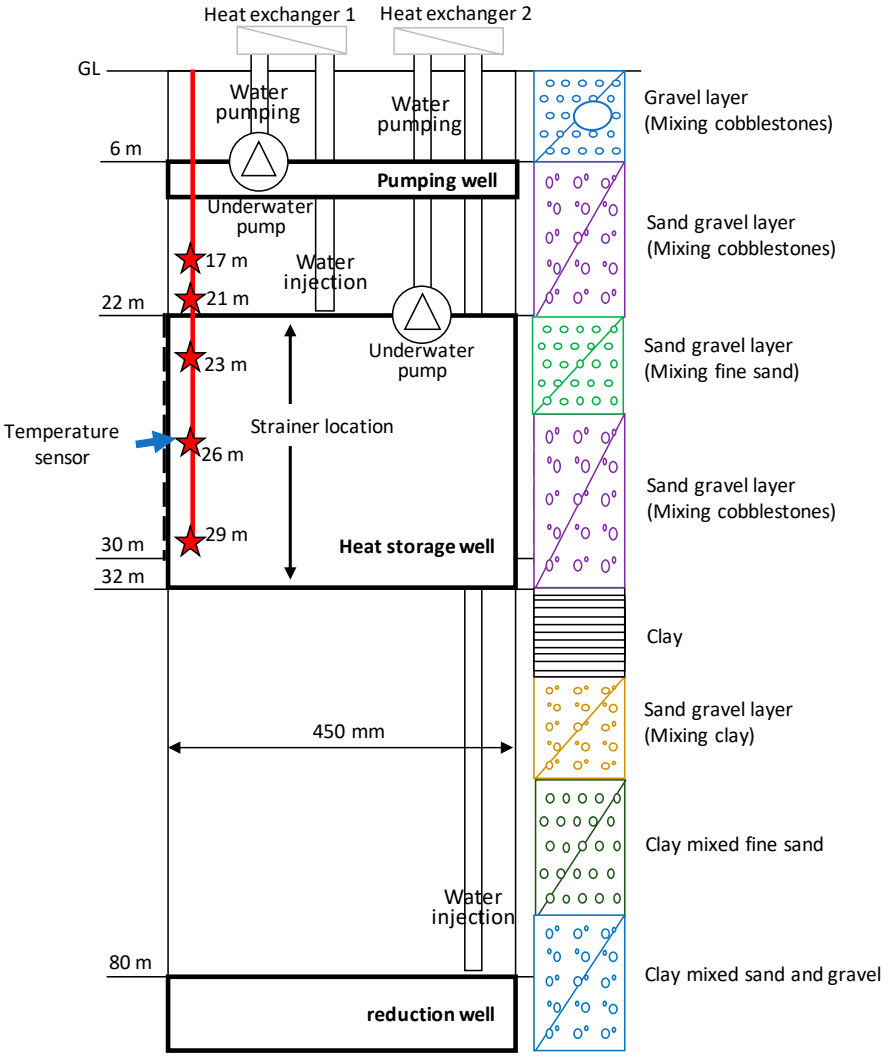

Figure 3. The stratum diagram of the heat storage well.

The accuracy of the aquifer model was verified using the measured data. Figure 4 shows the results of verifying the accuracy of the aquifer model. The measured data in Figure 4 represents the data measured at 23 m in the aquifer. The measured temperature between 17 m and 22 m is affected by the heat generated by the pump, while the temperature between 26 m and 29 m shows little change due to its depth. We will verify the accuracy of the simulation using the data at 23 m where we can see the temperature change between water injection and pumping. The aquifer model has errors between actual measurement and simulation due to water left in the pipes during the start-up operation. In addition, the trend differs from the measured values because the losses in the piping and the start-up and shutdown of the heat source equipment are not taken into account. The aquifer model was validated using root mean square error (RMSE). In the RMSE for summer operation, the water injection operation is 0.2 °C and the pumping operation is 0.8 °C. The summer operation reproduces the actual measured values. In the RMSE for winter operation, the water injection operation is 4.8 °C and the pumping operation is 2.2 °C. The winter operation reproduces the measured values except for the start of operation, although there are some differences from the measured values. In this model, the measured values can be reproduced in general except for about 30 min after the start of the calculation.

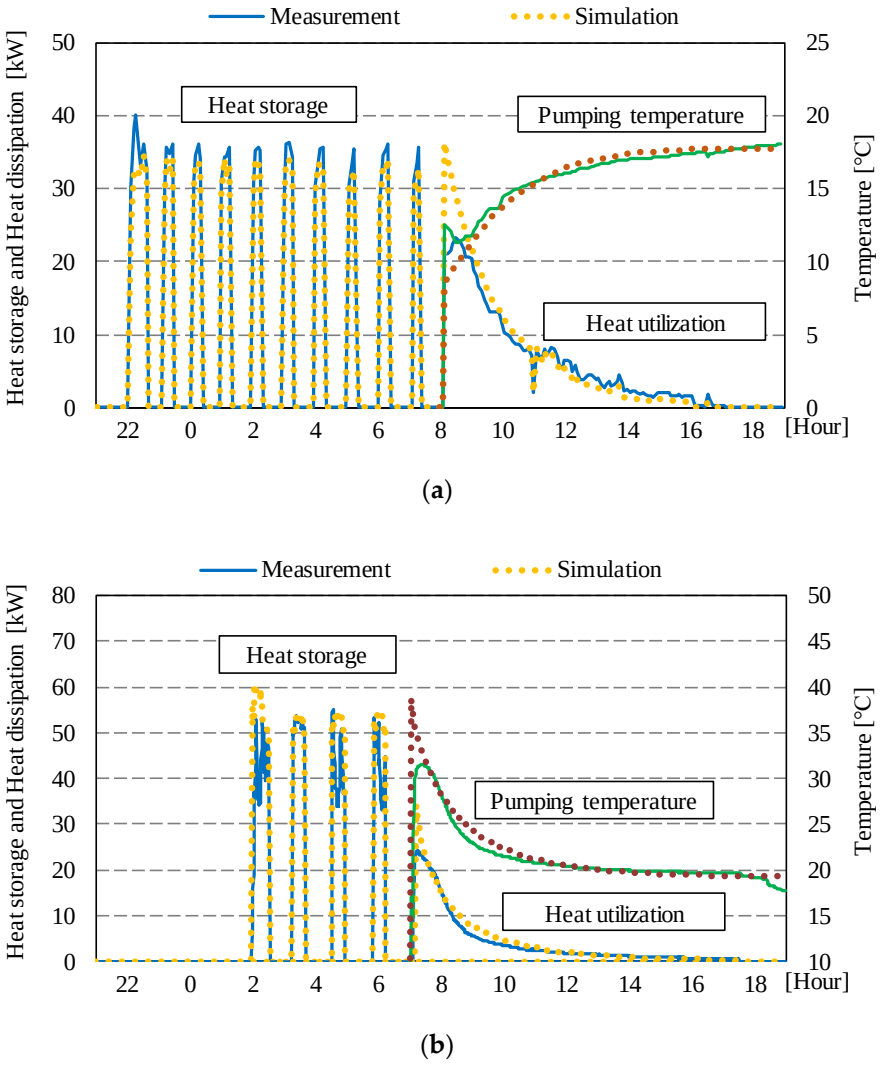

Figure 4. Accuracy verification of aquifer model. (**a**) Summer operation. (**b**) Winter operation.

3. Building Overview and Air Conditioning System

Table 2 shows the appearance and outline of the target building. The target building is an office building with five floors above ground and one floor of the tower. The system diagram of the air conditioning system installed in the target building is shown in Appendix C. BEMS is used to collect operation data of air conditioning systems. Figure 5 shows the transition of the load on the secondary side using BEMS data. The secondary load is calculated by the following Formula (1) using the secondary cold/hot water inlet/outlet temperature and flow rate of the BEMS data. The cooling load in summer is large, and the heating load in winter is smaller than the cooling load in summer. The load has a different pattern on weekdays and holidays, and changes according to the outside air temperature.

$$Q_{Heat\ Load} = m \times \rho \times c_p \times (t_{in} - t_{out}) \quad (1)$$

where $Q_{Heat\ Load}$ is the processing load [W], m is the flow rate of cold/hot water [m^3/s], ρ is the density of water [kg/m^3], c_p is the specific heat of water [J/(kg °C)], t_{in} is the water supply temperature [°C], t_{out} is the return water temperature [°C].

Table 2. Building overview.

Location	Takamatsu City, Japan
Site area	14,058.0 [m^2]
Total floor area	11,613.3 [m^2]
Building area	4278.2 [m^2]
Use	Office
Number of floors	5 floors above ground 1 floor of the tower
Outer wall	0.528 [W/m^2 K]
Roof	0.491 [W/m^2 K]
Window	2.40 [W/m^2 K] (Low-E glass)
Floor	0.753 [W/m^2 K]
Lighting	25 [W/ m^2]
Number of people in the room	0.15 [people/m^2]
ventilation rates	0.5 [times/h]

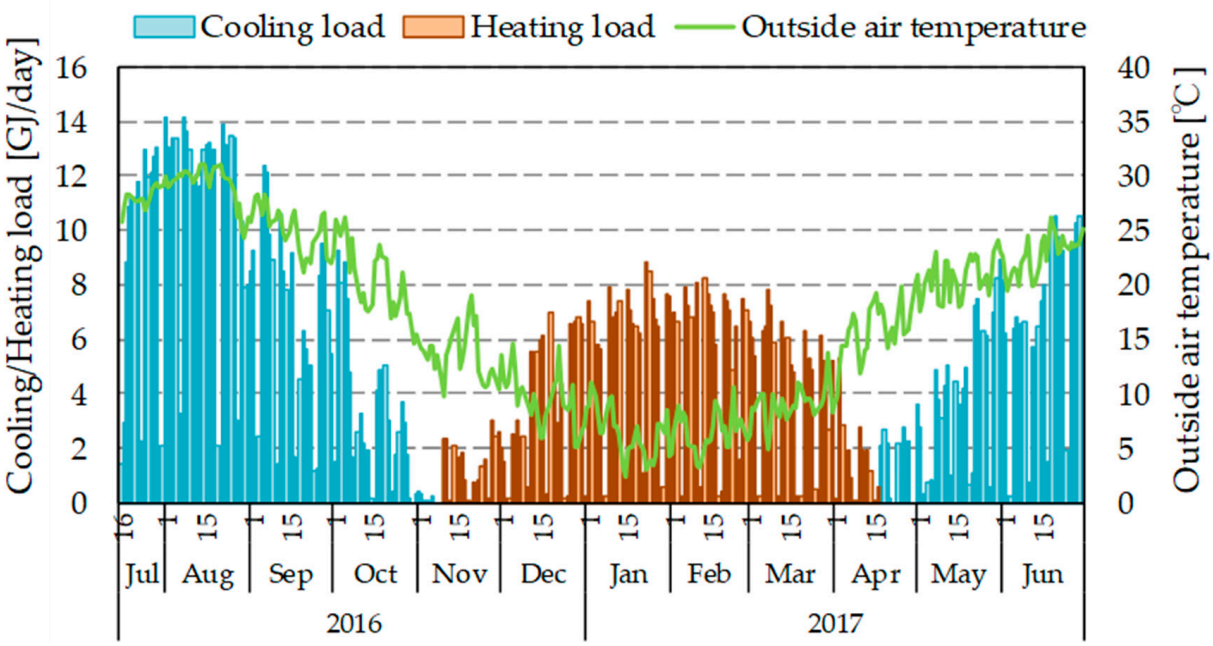

Figure 5. The cooling load and heating load and the outside air temperature of the building.

Figure 6 shows the transition of the air inlet temperature of the AHU installed in the room of the target building. Figure 6a shows the AHU air inlet temperature in summer. The hottest August outside air temperature is about 25 °C to 35 °C, and the AHU air inlet temperature is about 26 °C to 28 °C. Figure 6b shows the AHU air inlet temperature in winter. The coldest January outside air temperature is about 0 °C to 10 °C, and the AHU air inlet temperature is about 20 °C to 22 °C.

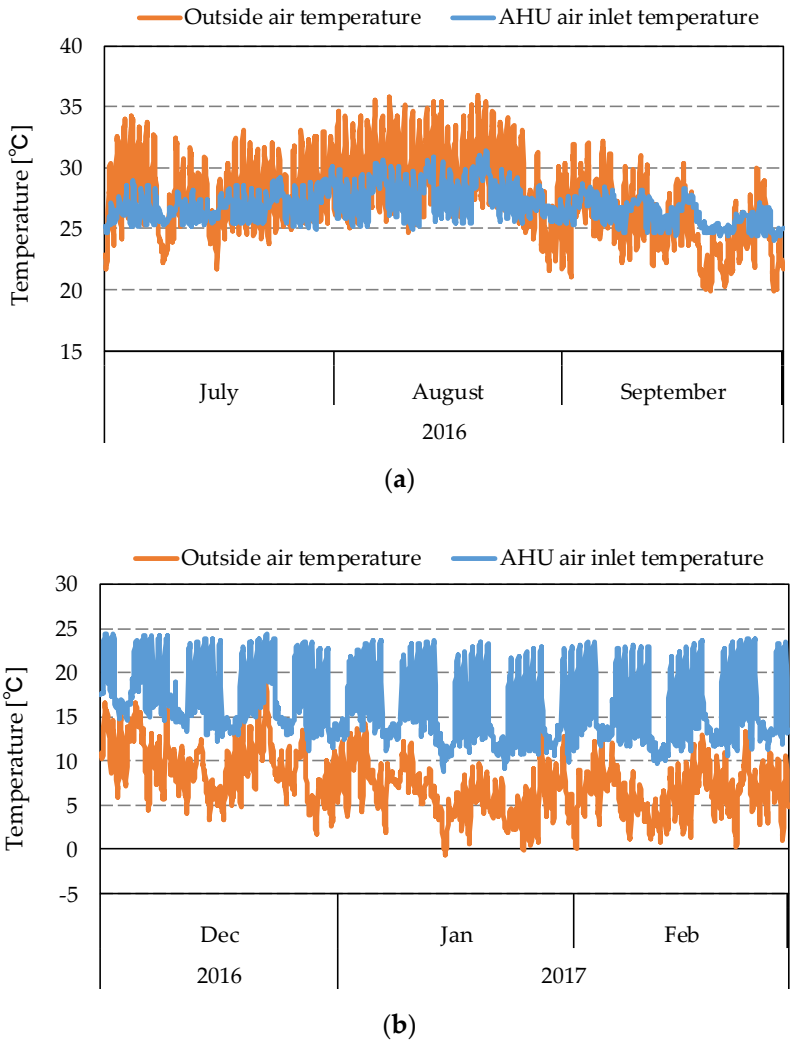

Figure 6. AHU inlet air temperature and outside air temperature. (**a**) The indoor temperature in summer and outside air temperature. (**b**) The indoor temperature in winter and outside air temperature.

4. An Efficient Operation Method of Aquifer Heat Storage System

Figure 7 shows the schematic diagram of the air conditioning system according to each case and operation method in this study. Table 3 shows the rated capacity of the heat pump and heat exchanger. In this study, a schematic diagram of the air conditioning system introduced by AHU was assumed throughout the building. The heat source equipment introduced a water-cooled heat pump and aquifer heat storage system. Three heat source devices have been introduced, two for nighttime heat storage and one for daytime operation.

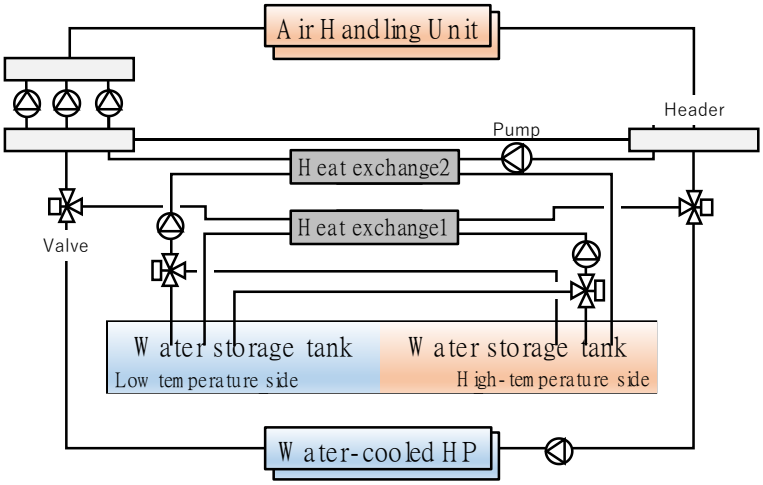

(**a**)

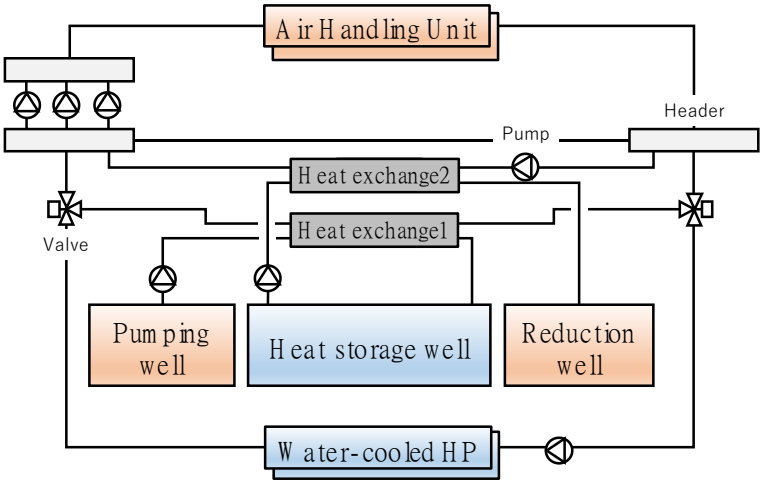

(**b**)

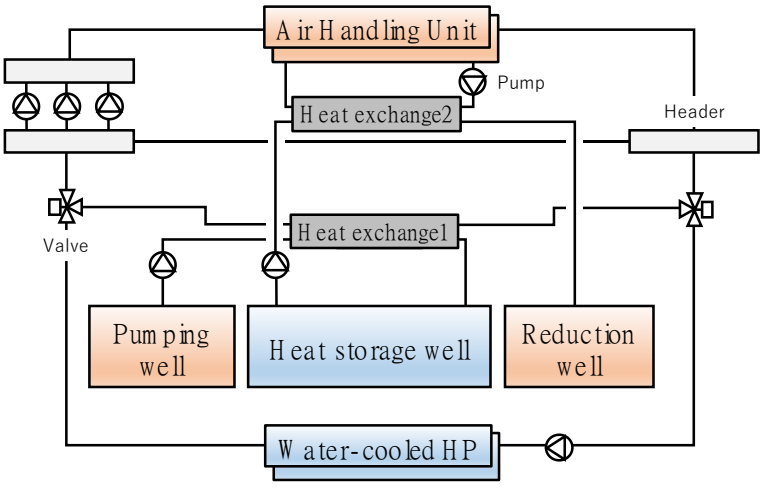

(**c**)

Figure 7. Air conditioning system diagram in each system. (**a**) WTES system. (**b**) ATES system. (**c**) ATES system (pre-cooling/pre-heating).

Table 3. The rated capacity of the heat source equipment.

Heat Source Equipment	Rated Capacity		Number of Units
Water-cooled HP	Cooling capacity [kW]	194.2	3
	Heating capacity [kW]	291.5	
Heat Exchanger 1	Heat exchange capacity [kW]	292.0	1
Heat Exchanger 2	Heat exchange capacity [kW]	210.0	1

In this study, we assume three types of cases. Figure 7a is a WTES system, which exchanges cold/hot water sent to the secondary side by a heat exchanger and cold/hot water from the heat storage tank. Figure 7b is an ATES system that sends heat to the secondary side in the same way as in Figure 7a. In Figure 7b, only the part of the water heat storage tank in Figure 7a is replaced with the ATES system, and the other configurations are the same. Figure 7c is an ATES system, in which heat is dissipated by the AHU pre-cooling/pre-heating coil installed on the secondary side. In Figure 7c, a pre-cooling/pre-heating coil that uses cold/hot water sent from the ATES system and a cold/hot water coil that uses cold/hot water sent from the water-cooled HP are introduced in the AHU. Figure 8 shows the configuration of the AHU.

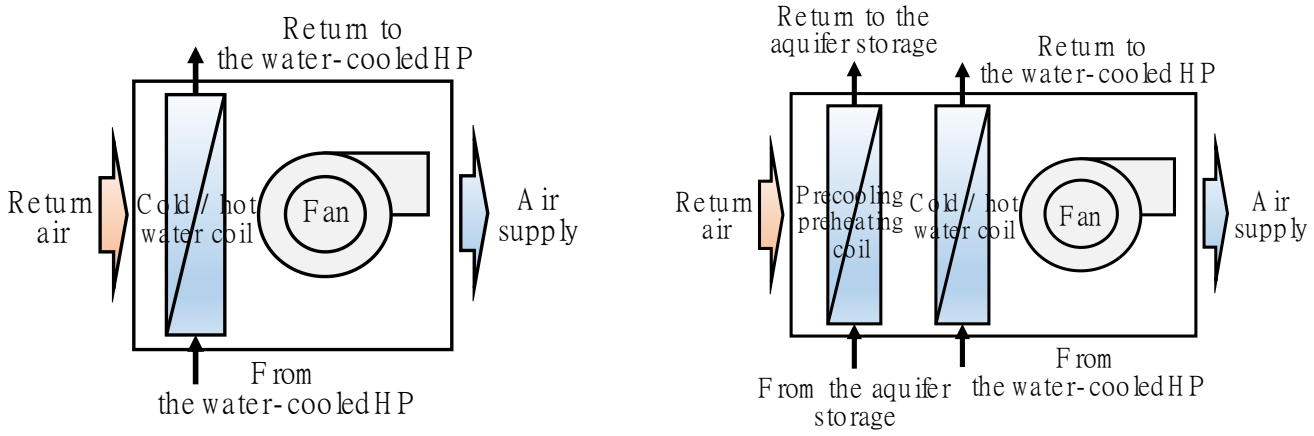

Figure 8. Configuration of the AHU. (**a**) Cold/Hot water coil. (**b**) Pre-cooling/Pre-heating coil.

Table 4 shows the cooling and heating operation cases. Case WTES is a WTES system operation, and Case ATES is an ATES system operation. C is a cooling operation, and H is a heating operation. The numbers divide the heat storage temperature. Case WTES is a case that reproduces the operation of a WTES system, and stores heat at a heat storage temperature of 7 °C for cooling operation and 45 °C for heating operation. Case ATES stores the ATES system at the same operation case as the WTES system, with the heat storage temperature at 7 °C for cooling operation and 45 °C for heating operation. CaseATES-C2 is a case in which a pre-cooling/pre-heating coil is provided in the AHU to search for a more suitable operation method for the ATES system (Figure 7c). Case ATES-C2 is divided into Case ATES-C2-7 and Case ATES-C2-14 according to the temperature level at which heat is stored.

Table 4. Cooling and heating operation case.

Air Conditioning Operation	Case	Heat Storage System	Operation Control and Method
Cooling operation	Case WTES-C1-7	WTES system operation	Cold water operation 7 °C heat storage operation
	Case ATES-C1-7	ATES system operation	Cold water operation 7 °C heat storage operation
	Case ATES-C2-7		Pre-cooling operation 7 °C heat storage operation
	Case ATES-C2-14		Pre-cooling operation 14 °C heat storage operation
Heating operation	Case WTES-H1-45	WTES system operation	Hot water operation 45 °C heat storage operation
	Case ATES-H1-45	ATES system operation	Hot water operation 45 °C heat storage operation
	Case ATES-H2-30		Pre-heating operation 30 °C heat storage operation
	Case ATES-H2-25		Pre-heating operation 25 °C heat storage operation
Heat storage operation time: 10 h Heat utilization operation time: 10 h Stop operation time: 4 h Initial groundwater temperature: 19.1 °C Initial storage tank temperature: 15 °C			

In each case, the heat storage operation is 10 h, the heat utilization operation is 10 h, and the operation stop is 4 h. The initial temperature of the aquifer is 19.1 °C, and the temperature of the water storage tank is 15 °C. The water-cooled HP of the heat source equipment operates the outlet temperature at 7 °C for cooling operation and 45 °C for heating operation. Case studies will be conducted using BEMS data from July to September for cooling operations and from December to February for heating operations. In the simulation of heat storage operation, a one-month run-up period is provided to stabilize the actual temperature change of the heat storage layer. The capacity of the ATES system and the WTES system is assumed to be 50% of the maximum building load, and the thermal storage operation is performed at night. Therefore, we calculated the flow rate of the heat exchanger assuming 10 h of thermal storage operation. Building load was analyzed using BEMS data. Building loads occurred from 8:00 to 18:00 in the summer and from 7:00 to 18:00 in the winter. The operation of the aquifer heat storage system and the water-cooled HP operates during the time when there is a building load. In the building load processing operation, the aquifer thermal storage system operates first, followed by the water-cooled HP.

5. Results and Discussions

5.1. Time of Day Analysis of Cooling and Heating Operations

Figure 9 shows the operation results on 9 August, when the secondary load of the cooling operation is the largest. In the HEX2 heat storage tank side inlet/outlet temperature transition in Figure 9a, Case WTES-C1-7 can send cold water of about 7 °C to 9 °C from the heat storage tank. In Case ATES-C1-7, the pumping temperature of the heat storage well has risen since 13:00, and heat exchange has not been possible since 16:00. An aquifer thermal storage system draws in groundwater from the surroundings as it pumps water from the aquifer. Therefore, heat is diffused in the aquifer, and it is difficult to maintain the temperature of the aquifer. The aquifer heat storage system is not suitable for use in the same way as the water heat storage system. Looking at the amount of heat stored and

dissipated in Figure 9b, it can be seen that Case ATES-C1-7 does not secure as much heat as Case WTES-C1-7 even though it stores more heat than Case WTES-C1-7.

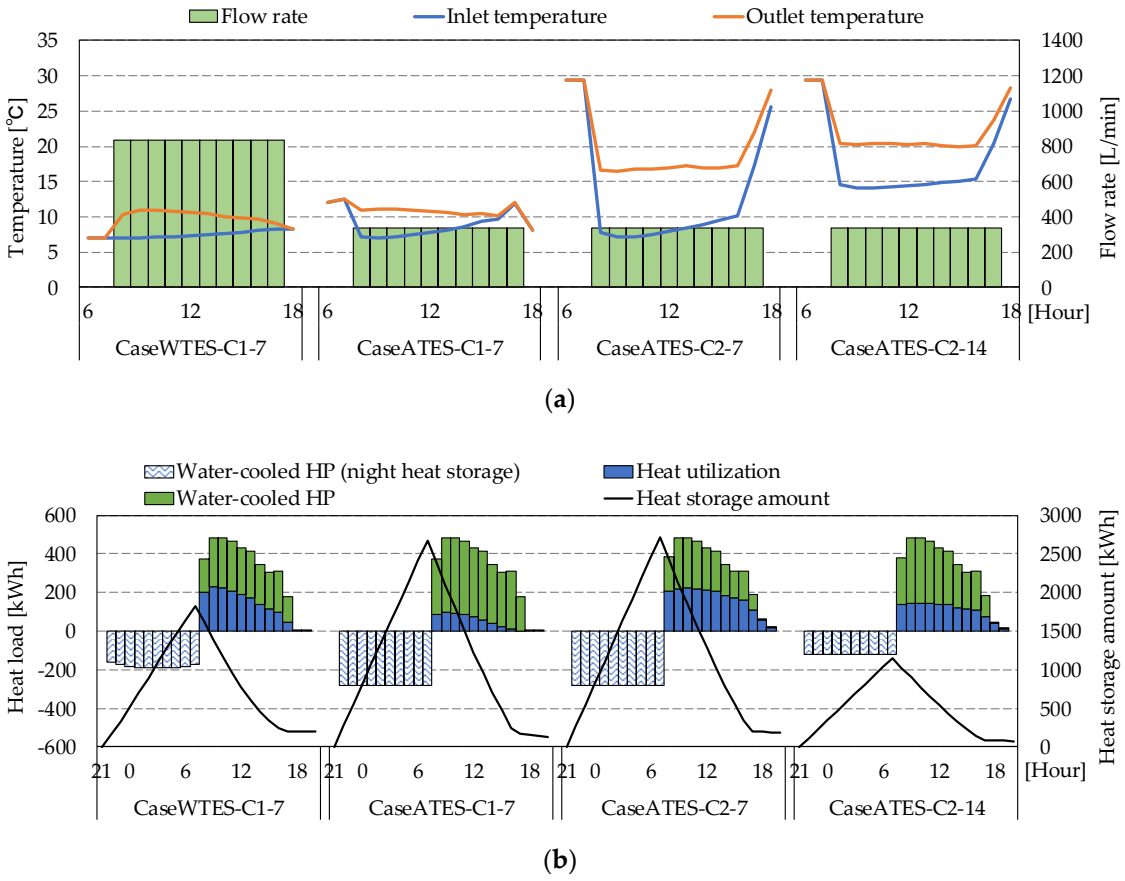

Figure 9. Operation analysis on 9 August in summer. (**a**) Flow rate and temperature of Heat Exchanger 2. (**b**) Operational transition of heat storage and heat utilization.

Case ATES-C2-7, which uses the heat of the aquifer heat storage system for pre-cooling operation, stores heat at 7 °C and supplies heat to the pre-cooling coil during heat utilization operation. In this case, the HEX2 heat storage tank side inlet temperature is about the same as Case ATES-C1-7, but the HEX2 heat storage tank side outlet temperature is kept high, and the inlet/outlet temperature difference can be secured. Looking at the amount of heat released in Figure 9b, the amount of heat released is about the same as Case WTES-C1-7. However, the amount of heat storage is larger than Case WTES-C1-7. Case ATES-C2-14 specializes in raising the temperature level for heat storage to 14 °C and supplying cold heat for pre-cooling. The HEX2 heat storage side inlet temperature is stable at 14 °C to 15 °C, and the temperature difference from the HEX2 heat storage side outlet temperature can be secured. The HEX2 heat storage side outlet temperature is about 20 °C, which is higher than the groundwater temperature of 19.1 °C originally in the aquifer. Therefore, the heat of groundwater can be used for air conditioning. From Figure 9b, it can be seen that the heat utilization amount of Case ATES-C2-7 is smaller than that of Case WTES-C1-7, but it is secured to some extent, and the heat storage amount is suppressed compared to Case WTES-C1-7. Looking at the transition of the heat storage amount of Case ATES-C2-14, the stored heat is almost used up at 18:00.

The heating operation on 23 January is shown in Figure 10. In the HEX2 heat storage tank side inlet/outlet temperature transition in Figure 10a, Case WTES-H1-45 can send hot water of about 45 °C to 42 °C from the heat storage tank. In Case ATES-H1-45, which is used in the same way as Case WTES-H1-45, the pumping temperature of the heat storage well drops to 42 °C after 11:00, and heat exchange is not possible from 11:00. As with

cooling operations, it is difficult to maintain a high temperature in the aquifer due to the influence of groundwater flowing in from the surroundings when water is pumped from the aquifer. Case ATES-H2-30 and Case ATES-H2-25 used for pre-heating operations are operating until 17:00. In Case ATES-H2-25, the temperature difference between the inlet and outlet on the HEX2 heat storage tank side has become smaller since 14:00. Case ATES-H2-25 specializes in lowering the temperature level for heat storage to 25 °C and supplying it for pre-heating. The HEX2 heat storage side inlet temperature is stable at 25 °C to 23 °C, and the temperature difference from the HEX2 heat storage side outlet temperature can be secured. The HEX2 heat storage side outlet temperature is about 22 °C. It can be seen that Case ATES-H1-45 in Figure 10b does not secure as much heat utilization as Case WTES-H1-45, even though it stores more heat than Case WTES-H1-45. The amount of heat stored in Case ATES-H2-25 is smaller than that of Case WTES-H1-45, but it is secured to some extent, and the amount of heat released is smaller than that of Case WTES-H1-45. In the transition of the heat storage amount of Case ATES-H2-30 and Case ATES-H2-25, the stored heat is almost used up at 17:00.

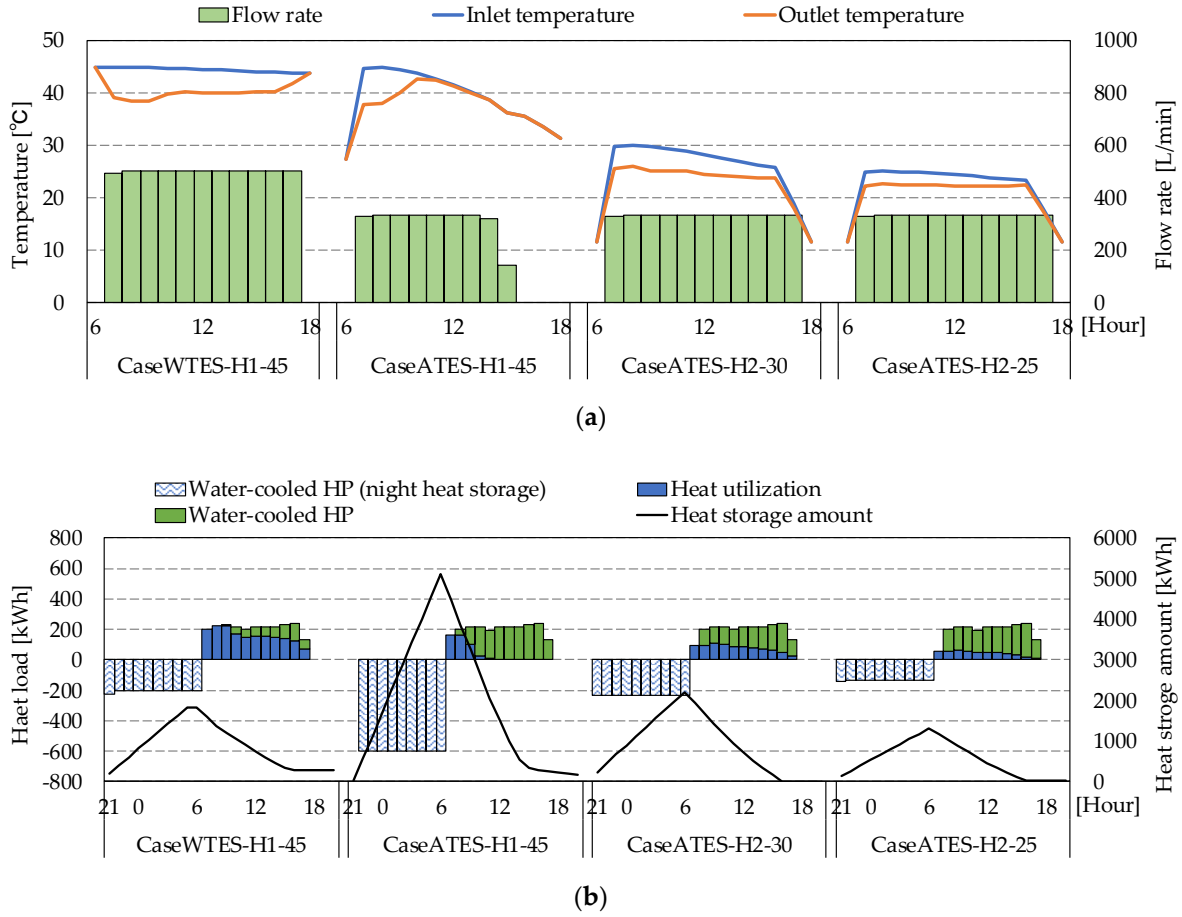

Figure 10. Operation analysis on 23 January in winter. (**a**) Flow rate and temperature of Heat Exchanger 2. (**b**) Operational transition of heat storage and heat utilization.

5.2. Analysis of AHU Inlet/Outlet Temperature and Humidity

Figures 11 and 12 show the operating trends of inlet and outlet temperature and humidity of AHU for heating and cooling operation. Figure 11 shows the air temperature and humidity before and after the AHU pre-cooling coil and chilled water coil in Case ATES-C1-7 and Case ATES-C2-14. The cold-water coil air outlet humidity of Case ATES-C1-7 and Case ATES-C2-14 is close to 100%. It can be seen that the cold-water coil is dehumidifying. In Figure 11b, the pre-cooling coil air outlet temperature is about 22 °C,

and the air humidity at this time is 60% to 80% except immediately after the start of operation. For this reason, the outlet of the pre-cooling coil is not in a dehumidified state, and only sensible heat is processed. If a pre-cooling coil is installed and the heat of the aquifer is used for air cooling up to a little over 20 °C, the heat storage temperature level of the aquifer can be raised, which leads to effective utilization of the groundwater heat.

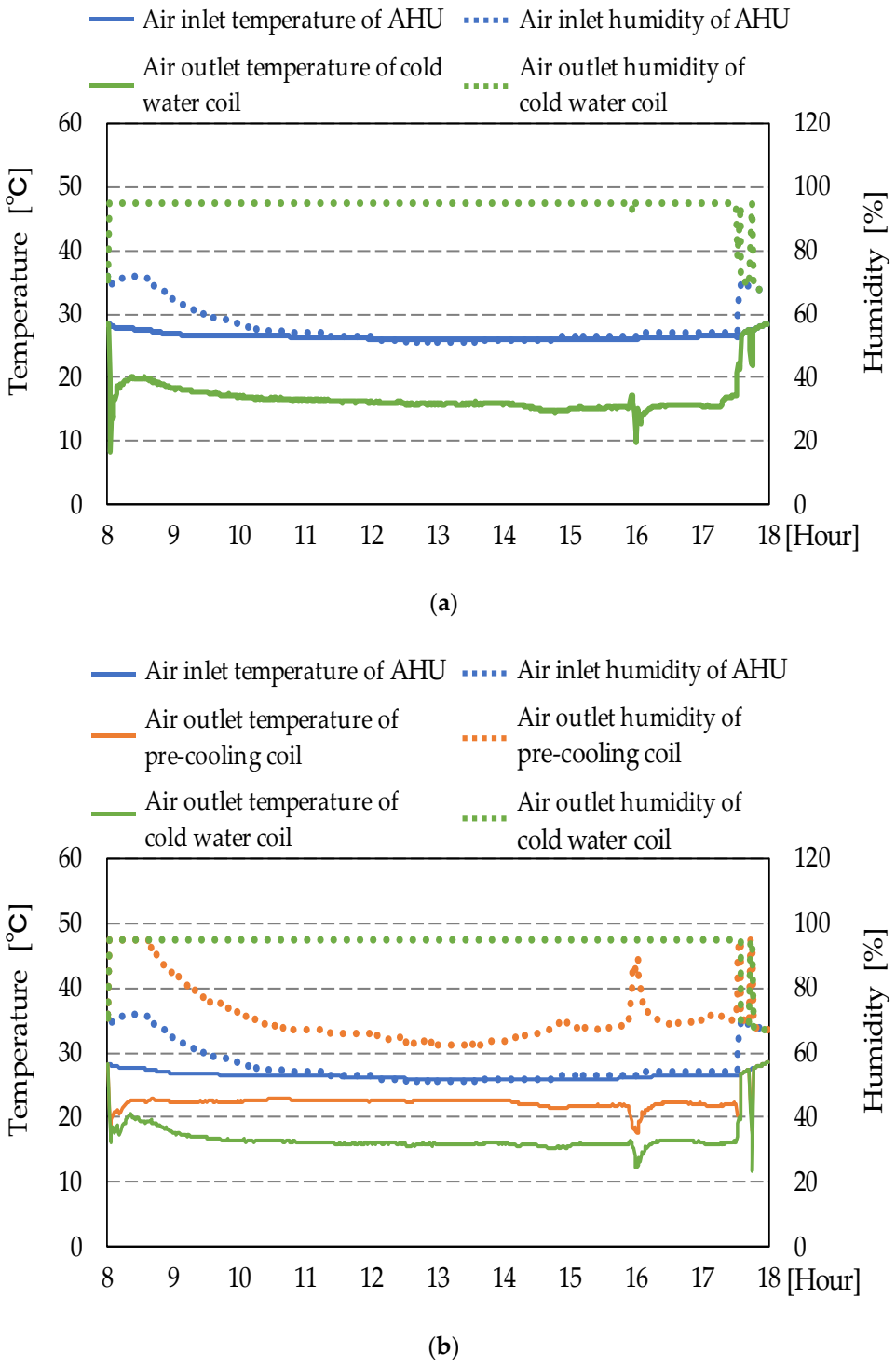

Figure 11. Air temperature and humidity before and after the AHU by the cooling operation. (**a**) Cold water coil operation (Case ATES-C1-7). (**b**) Pre-cooling coil operation (Case ATES-C2-14).

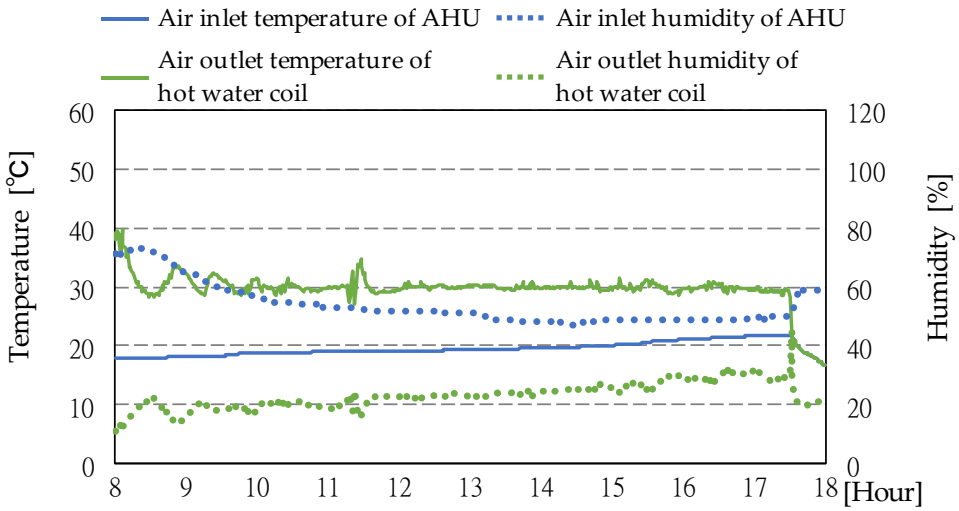

Figure 12. Air temperature and humidity before and after the AHU by the heating operation. (**a**) Hot water coil operation (Case ATES-C1). (**b**) Pre-heating coil operation (Case ATES-C2-2).

Figure 12 shows the air temperature and humidity before and after the AHU pre-heating coil and hot water coil in Case ATES-H1-45 and Case ATES-H2-25. The temperature of the hot water coil air outlet of Case ATES-H1-45 and Case ATES-H2-25 is controlled at about 30 °C. In Case ATES-H2-25 in Figure 12b, the pre-heating effect due to the operation of the ATES system has almost disappeared from around 15:00, and the pre-heating coil has not been able to heat it. The AHU air inlet temperature is about 19 °C, and the pre-heating coil heats it to about 22 °C. For pre-heating, it is sufficient to have hot water of at least 19 °C or higher, and it can be seen that it can be operated even if the heat storage temperature level of the aquifer is lowered. The AHU air inlet temperature of 19 °C is close to the under-ground temperature, and it is somewhat difficult to use the heat of groundwater as it is during heating.

5.3. Daytime Processing Heat and Total Power Consumption

Figures 13 and 14 shows a scatter plot of the ratio of heat-processed in water-cooled HP operation and the rate of increase in total power consumption. The scatter plot shows each case monthly. The lower the ratio of heat-processed in water-cooled HP operation, the more the building load is processed by the heat utilization operation. In addition, the heat storage system suppresses the peak in the daytime. The ratio of processing heat for water-cooled HP operation is calculated by Equation (2), and the rate of increase in total power consumption is calculated by Equation (3). The ratio of heat-processed by water-cooled HP operation is the ratio of building load processed using water-cooled HP. The rate of increase in total power consumption is the result of comparing the power consumption of each case with the water-cooled HP operation case. Power consumption includes power consumption of heat source equipment and pumps.

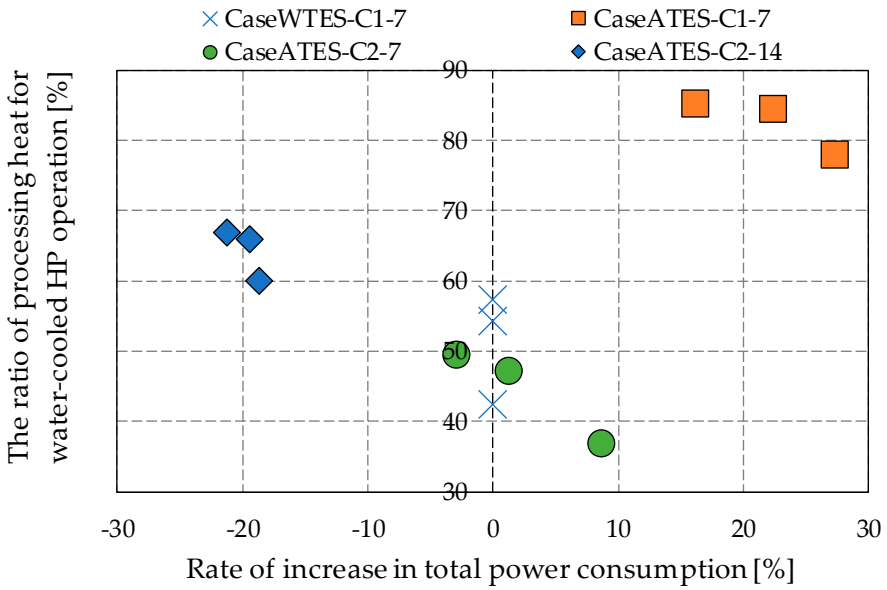

Figure 13. Processing heat ratio of the water-cooled HP in cooling operation and rate of increase in total power consumption.

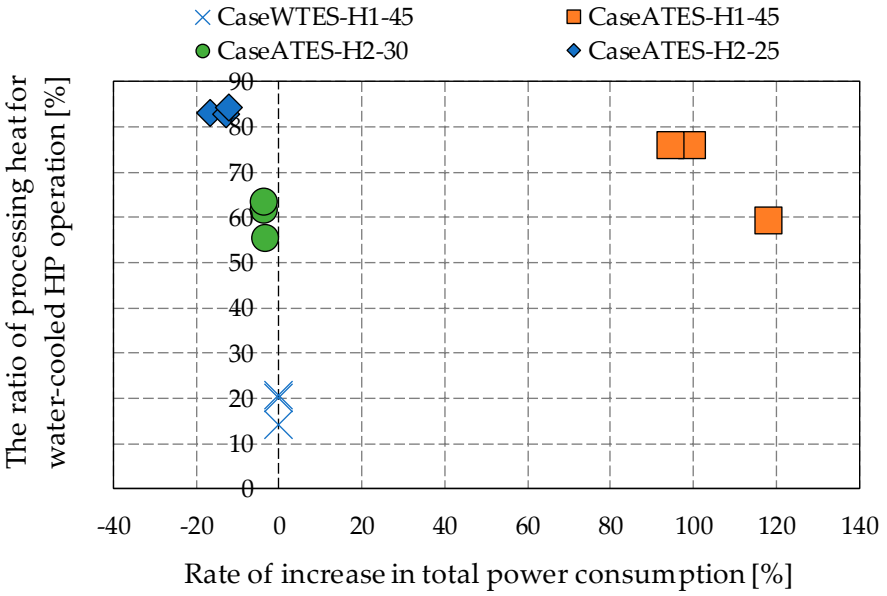

Figure 14. Processing heat ratio of the water-cooled HP in heating operation and rate of increase in total power consumption.

Figure 13 shows the Case WTES-C1-7 and Case ATES-C2-7 have a low the ratio of heat processed in water-cooled HP operation and suppress daytime power consumption. Case ATES-C2-7 has the same ratio of heat-processed in water-cooled HP operation and total power consumption as Case WTES-C1-7. Case ATES-C2-14 has a ratio of heat-processed in water-cooled HP operation of 10% to 20% point (pt) higher than Case WTES-C1-7. Total power consumption is reduced by 20%. Case ATES-C1-7 has a higher ratio of heat-processed in water-cooled HP operation and total power consumption than Case WTES-C1-7.

Figure 14 shows the processing heat ratio of Case WTES-H1-45 in water-cooled HP operation is low, and daytime power consumption is suppressed. Figure 14 shows the Case WTES-H1-45 has a low ratio of heat-processed in water-cooled HP operation and suppresses daytime power consumption. Case ATES-H2-30 has a higher ratio of heat-processed in water-cooled HP operation of 40% to 50% pt than Case WTES-H1-45. Case ATES-H2-25 is 60% pt higher. Case ATES-H2-30 and Case ATES-H2-25 have a lower nighttime heat storage temperature than Case WTES-H1-45. Therefore, the power consumption of the nighttime heat storage operation is reduced, and the total power consumption is reduced. Since the room temperature in winter is the same as the aquifer temperature, it was difficult to operate the pre-heating coil.

$$Q_{rate} = \frac{Q_{W\_HP}}{Q_{Load}} \times 100 \quad (2)$$

$$W_{rate} = \frac{W_{ATES}}{W_{W\_HP}} \times 100 \quad (3)$$

where Q_{rate} is the ratio of processing heat for water-cooled HP operation [%], Q_{W_HP} is processing heat of water-cooled HP [kW], Q_{Load} is building load [kW], W_{rate} is rate of increase in total power consumption [%], W_{W_HP} is water-cooled HP power consumption [kW], W_{ATES} is ATES system power consumption [kW].

Figure 15 shows the power consumption and energy efficiency. Table 5 shows the seasonal power consumption and energy efficiency. The coefficient of performance (COP) is calculated by Equation (5), the energy efficiency ratio (EER) is calculated by Equation (6), and the seasonal energy efficiency ratio (SEER) is calculated by Equation (7.) The COP is the ratio of the heating or cooling output power to the input power demand of the heat pump. The EER is calculated by multiplying the COP by 3.413. EER values of higher 8.5 are efficient. A higher EER rating means that of cooling effect for every Watt of energy you provide. The SEER is the ratio of the total cooling of the heat pump to the total electrical energy input during the same period. SEER values of 8–10 are efficient.

Table 5. Seasonal power consumption and energy efficiency.

Case	Operation	Power Consumption [MWh]	COP [-]	EER [-]	SEER [-]
Case WTES-C1-7	Cooling	71.5	2.9	10.0	11.1
Case WTES-H1-45	Heating	43.7	2.4	8.3	8.8
Case ATES-C1-7	Cooling	86.8	2.4	8.2	8.7
Case ATES-H1-45	Heating	89.1	1.2	4.1	3.9
Case ATES-C2-7	Cooling	72.8	2.9	9.8	10.8
Case ATES-H2-30	Heating	42.3	2.5	8.6	9.2
Case ATES-C2-14	Cooling	57.3	3.7	12.4	15.3
Case ATES-H2-25	Heating	37.7	2.8	9.6	10.6

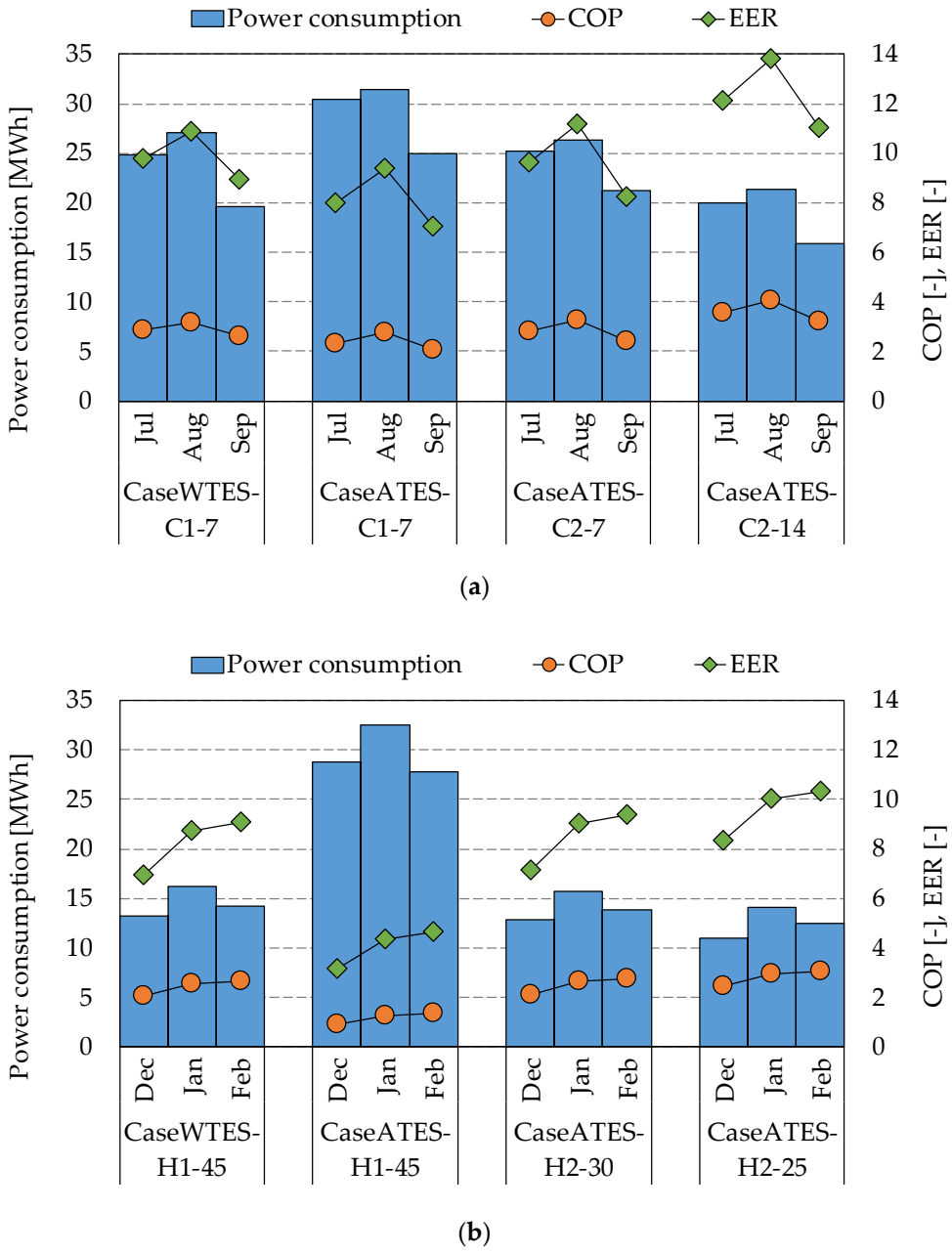

Figure 15. Power consumption and energy efficiency. (**a**) Summer operation. (**b**) Winter operation.

The COP for cooling operation was 2.4–3.7, with the ATES-C1-7 was the lowest at COP 2.4 and ATES-C2-14 was the highest at COP 3.7. The COP for heating operation is 1.2–2.8, with the ATES-H1-45 was the lowest at COP1.2, and in other cases, it was about the same at COP2.4-2.8. As mentioned in Chapter 5.1, the ATES system has difficulty maintaining heat for long periods. Therefore, it was found that the operation using the pre-cooling/pre-heating coil performs an efficient operation. In terms of energy efficiency, the heating operation ATES-H1-45 had a low energy efficiency of 4.1 for EER and 3.9 for SEER. In other cases, the energy efficiency was 8.2–12.4 for EER and 8.7–15.3 for SEER.

The COP of the ATES system operation in this study is about two lower than that of the ATES system coupled with a chiller for cooling operation in Ghaebi et al. [21]. The pre-cooling/pre-heating operations considered in this study have a similar SEER compared to the work of Vanhoudt et al. [22], Picone et al. [24]. However, it is about 10 lower than the summer SEER in Vanhoudt et al. [22]. In the Vanhoudt et al. [22] study, the aquifer

temperature is 10 °C lower than the aquifer temperature in this study, which is considered to be specialized for cooling operation.

$$COP = \frac{Output\ power}{Input\ power} \tag{4}$$

$$EER = 3.413 \times COP \tag{5}$$

$$SEER = \frac{Total\ seasonal\ cooling\ output}{Total\ electrical\ energy\ input} \tag{6}$$

where COP is the coefficient of performance of heat pump [-], $output\ power$ is the power drawn from the heat pump as cooling or heat [W], $input\ power$ is the power supplied to the compressor [W], EER is an energy performance rating for cooling devices [-], $SEER$ is the seasonal cooling performance [-], $total\ seasonal\ cooling\ output$ [Wh], $total\ electrical\ energy\ input$ [Wh].

6. Conclusions

In this study, we compared the operating performance of the WTES system of the existing heat storage system and the ATES system using a simulation model and clarified the efficient operation method of the ATES system. This study uses three aquifers: pumping wells, thermal storage wells, and reducing wells. The initial temperature is 19.1 °C groundwater from the surrounding area. The findings obtained in this study are summarized below.

(1) In the ATES system, if the same operation method as the WTES system is used, the heat storage efficiency will decrease, and the energy consumption will increase.
(2) When using an ATES system, the cold and hot heat input to the aquifer diffuses quickly and the pumping temperature changes quickly, it is suitable to introduce a pre-cooling and pre-heating coil. That allows heat to be used even when the water temperature approaches the underground temperature.
(3) The aquifer heat storage system was used for the pre-cooling coil, and the cooling power consumption was reduced by 20%. If a pre-cooling/pre-heating coil is introduced and energy saving is important, heat is stored at a low temperature close to the geothermal temperature, and the operation that also uses the groundwater heat is performed. In addition, if the reduction of peak power in the daytime is important, it is appropriate to operate so that the heat stored in the pre-cooling/pre-heating coil is used up as much as possible.
(4) In cooling operation, ATES-C1-7 was the lowest at COP 2.4 and ATES-C2-14 was the highest at COP 3.7. In heating operation, ATES-H1-45 was the lowest at COP1.2, and in other cases, it was about the same at COP2.4-2.8.
(5) In terms of energy efficiency, the heating operation ATES-H1-45 had a low energy efficiency of 4.1 for EER and 3.9 for SEER. In other cases, the energy efficiency was 8.2–12.4 for EER and 8.7–15.3 for SEER.

Author Contributions: All authors contributed to the study conception and design; writing—original draft preparation, J.O.; writing—review and editing, J.O., H.K. and D.S.; supervision, D.S.; project administration, D.S.; methodology, M.N.; formal analysis, M.N. All authors have read and agreed to the published version of the manuscript.

Funding: This research received no external funding.

Institutional Review Board Statement: Not applicable.

Informed Consent Statement: Not applicable.

Data Availability Statement: Not applicable.

Acknowledgments: We wish to thank Shikoku Electric Power Co., Inc. and Yonden Consultants Co., Ltd. for their cooperation in advancing this research.

Conflicts of Interest: The authors declare no conflict of interest.

Appendix A

The equations for the heat balance of the WTES system model are shown in Equations (A1)–(A6).

- Heat utilization

Layer N $$V\frac{dT_N}{dt} = GW_{AC}(T_{AC} - T_N) \quad \text{(A1)}$$

Layer i $$V\frac{dT_i}{dt} = GW_{ST}(T_{i+1} - T_i) \quad \text{(A2)}$$

Layer 1 $$V\frac{dT_1}{dt} = GW_{ST}(T_2 - T_1) + GW_{MC}(T_{MC} - T_1) \quad \text{(A3)}$$

- Heat storage

Layer 1 $$V\frac{dT_1}{dt} = GW_{MC}(T_{MC} - T_1) \quad \text{(A4)}$$

Layer i $$V\frac{dT_i}{dt} = GW_{ST}(T_{i-1} - T_1) \quad \text{(A5)}$$

Layer N $$V\frac{dT_N}{dt} = GW_{ST}(T_{N-1} - T_N) + GW_{AC}(T_{AC} - T_N) \quad \text{(A6)}$$

where V is capacity of each layer [m^3], t is time [min], *GW_AC* is flow rate from secondary side [m^3/h], *GW_MC* is flow rate from heat source [m^3/h], *GW_ST* is flow rate between layers [m^3/h], *T_AC* is inflow temperature from secondary side [°C], *T_MC* is inflow temperature from heat source [°C], *T_i* is temperature of layer i [°C], *T_N* is temperature of layer N [°C]

Appendix B

For the aquifer model, parameters were set using experimental data. The root mean squared error (RMSE) was used for model evaluation [39]. In order to reproduce the actual aquifer, the dispersion length was set to 0.05 m and the thickness of the impermeable layer was set to 0.002 m. However, it is unlikely that such a thin impervious layer will exist. Figure A1 shows the sensitivity analysis. Sensitivity analysis was performed using previous studies to examine how much it affects the model [40]. The thickness of the impermeable layer represents the heat insulating performance of the aquifer. For the model parameters of this study, the model settings shown in Table A1 were set in order to assume the same performance as the water heat storage system.

Table A1. The ATES system model input values.

	Radius [m]	20
	Initial division width [m]	0.03
	common ratio [-]	1.10
Aquifer	Volumetric specific heat [MJ/(m^3K)]	3.18
	Effective thermal conductivity [W/(mK)]	1.6
	Clearance rate [-]	0.3
clay	Volumetric specific heat [MJ/(m^3K)]	3.06
	Effective thermal conductivity [W/(mK)]	1.2
	Clearance rate [-]	0.3
Water	Volumetric specific heat [MJ/(m^3K)]	4.18
	Thermal conductivity [W/(mK)]	0.59
	Aquifer thickness [m]	8
	Dispersion length [m]	0.05
	Impermeable layer thickness [m]	1
	Initial underground temperature [°C]	19.1

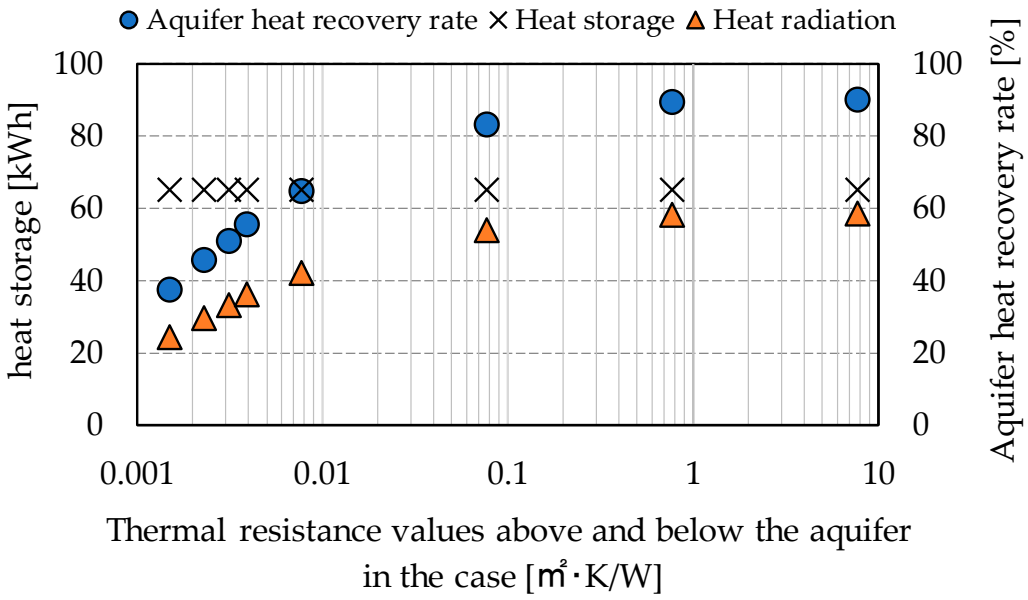

Figure A1. The sensitivity analysis of the model.

Appendix C

The target building has the air conditioning system diagram shown in Figure A2 and the specifications of the heat source equipment shown in Table A2. The air conditioning system uses BEMS to collect data. Air-cooled heat pumps (air-cooled HP), ice heat storage systems, water-cooled HP, and ATES systems have been introduced as heat source equipment. The secondary side processing the load of the building by the fan coil unit (FCU) and the AHU. In the air conditioning system of the subject building, the TES system operates first, followed by the water-cooled HP. Finally, the air-cooled HP is in operation control. On the secondary side, the AHU and FCU processing the building load.

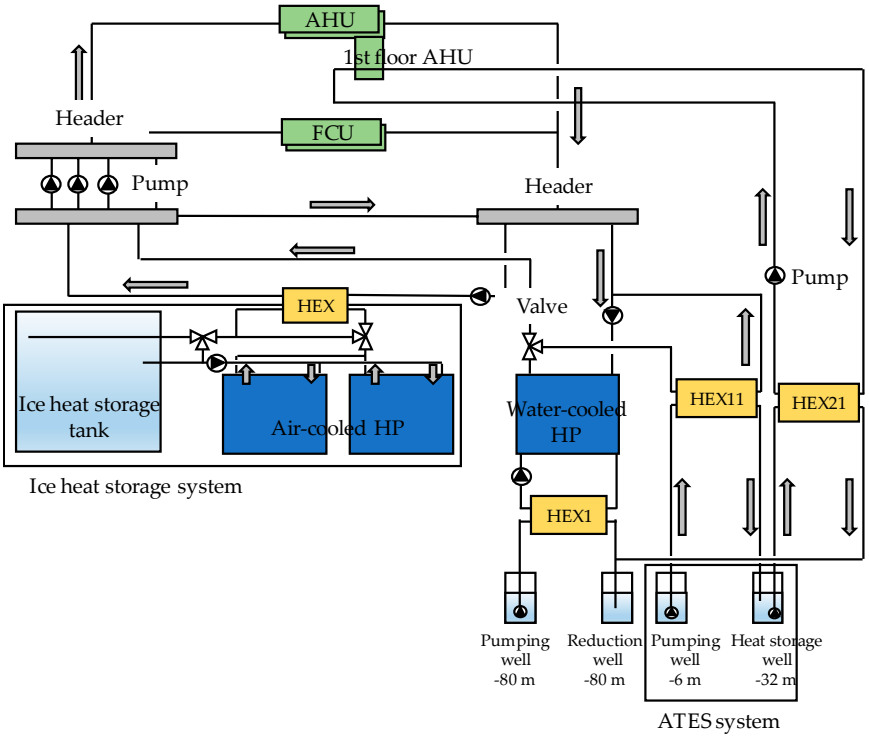

Figure A2. System diagram of the target air conditioning system.

Table A2. Specifications of heat source equipment.

Heat Source Equipment	Rated Capacity		Number of Units
Ice heat storage tank	Heat storage capacity [MJ]	4176 *1	1
	Heat storage capacity [kW]	120.1	
	Heat utilization capacity [kW]	116.0 *2	
Air-cooled HP	Cooling capacity [kW]	345.0	2
	Heating capacity [kW]	309.2	
Water-cooled HP	Cooling capacity [kW]	182.7	1
	Heating capacity [kW]	197.9	
Heat Exchanger 1	Cooling exchange heat quantity [kW]	157.0	1
	Heating exchange heat quantity [kW]	214.0	
Heat Exchanger 11	Cooling/heating exchange heat quantity [kW]	122.8	1
Heat Exchanger 21	Cooling/heating exchange heat quantity [kW]	35.0	1

*1 Calorific value of 10 h deicing operation; *2 capacity during 10 h heat utilization operation.

References

1. Ferrer, N.; Folch, A.; Lane, M.; Olago, D.; Odida, J.; Custodio, E. Groundwater hydrodynamics of an Eastern Africa coastal aquifer, including La Niña 2016–17 drought. *Sci. Total Environ.* **2019**, *661*, 575–597. [CrossRef] [PubMed]
2. Xu, J.; Wang, R.Z.; Li, Y. A review of available technologies for seasonal thermal energy storage. *Sol. Energy* **2014**, *103*, 610–638. [CrossRef]
3. Lund, H.; Mathiesen, B.V. Energy system analysis of 100% renewable energy systems—The case of Denmark in years 2030 and 2050. *Energy* **2009**, *34*, 524–531. [CrossRef]
4. de Bruijn, E.A.M.; Bloemendal, M.; ter Borgh, M.M.; Godderij, R.R.G.G.; Vossepoel, F.C. Quantifying the contribution of heat recharge from confining layers to geothermal resources. *Geothermics* **2021**, *93*, 102072. [CrossRef]
5. Palensky, P.; Dietrich, D. Demand Side Management: Demand Response, Intelligent Energy Systems, and Smart Loads. *IEEE Trans. Ind. Inform.* **2011**, *7*, 381–388. [CrossRef]
6. Lund, H. Large-scale integration of optimal combinations of PV, wind and wave power into the electricity supply. *Renew. Energy* **2006**, *31*, 503–515. [CrossRef]
7. Rostampour, V.; Jaxa-Rozen, M.; Bloemendal, M.; Keviczky, T. Building Climate Energy Management in Smart Thermal Grids via Aquifer Thermal Energy Storage Systems. *Energy Procedia* **2016**, *97*, 59–66. [CrossRef]
8. Sommer, W.; Valstar, J.; Leusbrock, I.; Grotenhuis, T.; Rijnaarts, H. Optimization and spatial pattern of large-scale aquifer thermal energy storage. *Appl. Energy* **2015**, *137*, 322–337. [CrossRef]
9. Takahashi, J.; Kondou, M.; Yokoo, N.; Oka, T. Analysis on the Co-efficient of Performance of Air Source Heat Pump Chiller System with Thermal Storage. *Soc. Heat. Air-Cond. Sanit. Eng. Jpn.* **1999**, *75*, 71–80. [CrossRef]
10. Figgener, J.; Stenzel, P.; Kairies, K.P.; Linßen, J.; Haberschusz, D.; Wessels, O.; Angenendt, G.; Robinius, M.; Stolten, D.; Sauer, D.U. The development of stationary battery storage systems in Germany—A market review. *J. Energy Storage* **2020**, *29*, 101153. [CrossRef]
11. Hesse, H.C.; Martins, R.; Musilek, P.; Naumann, M.; Truong, C.N.; Jossen, A. Economic Optimization of Component Sizing for Residential Battery Storage Systems. *Energies* **2017**, *10*, 835. [CrossRef]
12. Yang, T.; Liu, W.; Kramer, G.J.; Sun, Q. Seasonal thermal energy storage: A techno-economic literature review. *Renewable and Sustainable Energy Rev.* **2021**, *139*, 110732. [CrossRef]
13. Todorova, O.; Alannea, K.; Virtanena, M.; Kosonena, R. A method and analysis of aquifer thermal energy storage (ATES) system for district heating and cooling: A case study in Finland. *Sustain. Cities Soc.* **2020**, *53*, 101977. [CrossRef]
14. Bloemendal, M.; Jaxa-Rozen, M.; Olsthoorn, T. Methods for planning of ATES systems. *Appl. Energy* **2018**, *216*, 534–557. [CrossRef]
15. Ryu, Y.; Nishiyama, N.; Watanabe, T.; Akashi, Y. A Hybrid Energy Source System with Thermal Storage for Air Conditioning in a Middle Scale Office Building, Part 1 Outline of the HVAC System and Performance of a Shallow Temperature-Stratified Thermal Storage System. *Soc. Heat. Air-Cond. Sanit. Eng. Jpn.* **1995**, *59*, 163–173. [CrossRef]
16. Yamaguchi, H.; Yoshida, H. Development of Optimal Operation Schemes for HVAC Systems with a Thermal Storage Tank and Verification in Simulation Bases using Real Building Data. *Soc. Heat. Air-Cond. Sanit. Eng. Jpn.* **2005**, *105*, 1–11. [CrossRef]
17. Nishiyama, N.; Ryu, Y.; Watanabe, T.; Akashi, Y. A Hybrid Energy Source System with Thermal Storage for Air Conditioning in a Middle Scale Office Building Part 2—Evaluation on Energy Consumption and 0perating Cost. *Soc. Heat. Air-Cond. Sanit. Eng. Jpn.* **1996**, *60*, 51–61. [CrossRef]

18. Regenspurg, S.; Alawi, M.; Norden, B.; Vieth-Hillebrand, A.; Blöcher, G.; Kranz, S.; Scheytt, T.; Horn, F.; Burckhardt, O.; Rach, O.; et al. Effect of cold and hot water injection on the chemical and microbial composition of an aquifer and implication for its use as an aquifer thermal energy storage. *Geothermics* **2020**, *84*, 101747. [CrossRef]
19. Limberger, J.; Boxem, T.; Pluymaekers, M.; Bruhn, D.; Manzella, A.; Calcagno, P.; Beekman, F.; Cloetingh, S.; van Wees, J.D. Geothermal energy in deep aquifers: A global assessment of the resource base for direct heat utilization. *Renew. Sustain. Energy Rev.* **2018**, *82*, 961–975. [CrossRef]
20. Sendrós, A.; Urruela, A.; Himi, M.; Alonso, C.; Lovera, R.; Tapias, J.C.; Rivero, L.; Garcia-Artigas, R.; Casas, A. Characterization of a Shallow Coastal Aquifer in the Framework of a Subsurface Storage and Soil Aquifer Treatment Project Using Electrical Resistivity Tomography (Port de la Selva, Spain). *Appl. Sci.* **2021**, *11*, 2448. [CrossRef]
21. Ghaebi, H.; Bahadori, M.N.; Saidi, M.H. Different operational alternatives of aquifer thermal energy storage system for cooling and heating of a residential complex under various climatic conditions in Iran. *Sci. Iran.* **2019**, *26*, 1281–1292. [CrossRef]
22. Vanhoudt, D.; Desmedt, J.; Bael, J.V.; Robeynb, N.; Hoes, H. An aquifer thermal storage system in a Belgian hospital: Long-term experimental evaluation of energy and cost savings. *Energy Build.* **2011**, *43*, 3657–3665. [CrossRef]
23. Paksoy, H.O.; Andersson, O.; Abaci, S.; Evliya, H.; Turgut, B. Heating and cooling of a hospital using solar energy coupled with seasonal thermal energy storage in an aquifer. *Renew. Energy* **2000**, *19*, 117–122. [CrossRef]
24. Picone, S.; Bloemendal, M.; Pellegrini, M.; Hoekstra, N.; Andreu Gallego, A.; Rodriguez Comins, J.; Murrel, A. Novel combinations of aquifer thermal energy storage with solar collectors, soil remediation and other types of geothermal energy systems. In Proceedings of the European Geothermal Congress 2019, Den Haag, The Netherlands, 11–14 June 2019; Available online: https://www.researchgate.net/publication/335277098 (accessed on 27 June 2021).
25. Paksoy, H.O.; Gürbüz, Z.; Turgut, B.; Dikici, D.; Evliya, H. Aquifer thermal storage (ATES) for air-conditioning of a supermarket in Turkey. *Renew. Energy* **2004**, *29*, 1991–1996. [CrossRef]
26. Karim, A.; Burnett, A.; Fawzia, S. Investigation of Stratified Thermal Storage Tank Performance for Heating and Cooling Applications. *Energies* **2018**, *11*, 1049. [CrossRef]
27. Nakamura, M.; Shimizu, T.; Hokoi, S. SYSTEM CONCEPT AND CONFIRMATION OF THERMAL PERFORMANCE: Study on thermal energy storage system utilizing finite aquifer (Part 1). *J. Archit. Plan. Environ. Eng. AIJ* **2021**, *546*, 69–74. [CrossRef]
28. Nakamura, M.; Yamaoka, M.; Higuchi, M.; Hokoi, S. ENERGY SAVING PERFORMANCE AND ECONOMIC FEASIBILITY -Study on thermal energy storage system utilizing finite aquifer (Part2). *J. Archit. Plan. Environ. Eng. AIJ* **2002**, *554*, 41–46. [CrossRef]
29. Umemiya, H.; Shimawaki, S.; Kobayashi, H. Field Experiments of the Thermal Storage Utilizing Aquifer (Improvement in Thermal Recovery Factor and Payback of the Investment). *Jpn. Soc. Mech. Eng.* **1988**, *54*, 178–184. [CrossRef]
30. Umemiya, H.; Aoyagi, T. Basic Study of Aquifer Thermal Energy Storage (An Investigation of Ferric Colloidal Dam in an Aquifer). *Jpn. Soc. Mech. Eng.* **1991**, *57*, 3543–3550. [CrossRef]
31. Nakaso, Y.; Ito, T.; Sasaki, K.; Fujii, R.; Nakao, M.; Nishioka, M.; Nabeshima, M. Study on Daily Thermal Storage System using High Closure Aquifer (Part.1)—Experiment and Verification with ATES Model. *Soc. Heat. Air-Cond. Sanit. Eng. Jpn.* **2013**, *38*, 11–20. [CrossRef]
32. Nakaso, Y.; Sasaki, K.; Fujii, R.; Nakao, M.; Nishioka, M.; Nnabeshima, M. Study on Daily Thermal Storage System ufflizing High Closure Aquifer (Part.2)—Experiment alld Verification with ATES Model. *Soc. Heat. Air-Cond. Sanit. Eng. Jpn.* **2013**, *38*, 11–18. [CrossRef]
33. FEFLOW Manual. Available online: http://www.feflow.infouploadsmediauser_manual.pdf (accessed on 30 August 2021).
34. Kitaoka, T.; Kusumi, H.; Nakamura, M. 3D simulation analysis of groundwater seepage flow and thermal movement for energy conservation related with aquifer thermal energy storage. *Jpn. Geotech. Soc.* **2013**, *8*, 361–368. [CrossRef]
35. Ochifuji, K.; Suzuki, M.; Nakamura, M. Study of Seasonal Ground Heat Storage of Solar Energy Using a Vertical Pipe System Part 1—Introduction, Soil Temperature of Sapporo, Pipe Temperature. *Soc. Heat. Air-Cond. Sanit. Eng. Jpn.* **1985**, *10*, 13–24. [CrossRef]
36. Ochifuji, K.; Nakamura, M.; Nagano, K.; Ikenaga, Y.; Kobata, T. Investigation of the Long Term Heat Storage in the Aquifer. *Soc. Heat. Air-Cond. Sanit. Eng. Jpn.* **1992**, *17*, 53–61. [CrossRef]
37. Niwa, H.; Sagara, K.; Sekimoto, Y.; Inooka, T. Study on Optimization of Thermal Storage Performance for a Temperature Stratified Thermal Storage Tank. *Soc. Heat. Air-Cond. Sanit. Eng. Jpn.* **1994**, *19*, 57–68. [CrossRef]
38. Sagara, K.; Nakahara, N. Study on Heat Storage Water Tank Part—Estimation of Tank Efficiency for Stratified-type Tanks by System Simulation using Design of Experiments Method. *Soc. Heat. Air-Cond. Sanit. Eng. Jpn.* **1987**, *12*, 15–26. [CrossRef]
39. Oh, J.; Sumiyoshi, D.; Nishioka, M.; Kim, H. Efficient Operation Method of Aquifer Thermal Energy Storage System Using Demand Response. *Energies* **2021**, *14*, 3129. [CrossRef]
40. Oh, J.; Sumiyoshi, D.; Choi, Y.; Fujii, R.; Amano, Y.; Horioka, K.; Nishioka, M. Efficient Operation Method of an Aquifer Thermal Storage System: Analysis of operation efficiency by thermal resistance performance and precooled operation method. *Soc. Heat. Air-Cond. Sanit. Eng. Jpn.* **2021**, *287*, 1–12.